Assessment of the Flexural Bond Stresses of New Generation GFRP Bars

Jesús D. Ortiz, Zahid Hussain, Seyed-Arman Hosseini, Brahim Benmokrane and Antonio Nanni

Synopsis: As a result of the limited data available when the current ACI 440.11-22 development length equation was developed, certain parameters were disregarded. Additionally, the equation was based on bars that are no longer in use today, and significant advancements have been made in FRP material properties and production methods since its calibration. Conflicting research findings have led to differing perspectives on its reliability, with some suggesting it yields overly conservative results, while others argue it may overestimate bond strength. To address this concern, an experimental study was conducted to assess the bond stresses between GFRP bars and conventional concrete in underreinforced concrete beams. The beams were reinforced using a single M16 (No.5) Glass/Vinyl-ester FRP sand-coated bar. Three different lap splice lengths (i.e., 40-, 60-, and 80-times bar diameter) were selected based on available literature. The results indicate that the bond is primarily governed by surface friction, with negligible impact from relative slippage. The lap-spliced specimens exhibited slippage failure but exceeded design moments based on ACI provisions, indicating efficient performance. Stiffness remained comparable to that of the un-spliced beam, suggesting intact bond capacity despite some slippage. Average bond stress calculations closely aligned with ACI maximum bond stress values. Overall, the study offers valuable insights into GFRP bar behavior and bond capacity.

Keywords: bond failure, bond stresses, development length, GFRP rebars, rebar slippage.

ACI student member **Jesús D. Ortiz** is a PhD Candidate in the Civil and Architectural Engineering Department at the University of Miami. His research is focused on reinforcing, strengthening, and repair of concrete structures with FRP composites.

ACI student member **Zahid Hussain** is a PhD Candidate in Civil and Architectural Engineering Department at the University of Miami. His research interests include sustainable materials, computational methods, design methodology and behavior of FRP reinforced structures.

ACI student member **Seyed-Arman Hosseini** is a PhD candidate in the Civil Engineering Department at the University of Sherbrooke, QC, Canada. His research is focused on the behavior of FRP-reinforced concrete structures and sustainable design.

ACI fellow **Brahim Benmokrane** is Professor in the Department of Civil Engineering at the University of Sherbrooke (QC, Canada), Tier-1 Canada Research Chair Professor in Advanced Composite Materials for Civil Structures, and Senior Research Chair Professor in FRP Reinforcement for Concrete Infrastructure. He is a current member of ACI Committees 440 and 435. His research interests include the development of FRP reinforcement for concrete structures.

ACI fellow **Antonio Nanni** is Professor and Chair of the Department of Civil and Architectural Engineering at the University of Miami, FL. He has been an active member of many ACI committees, including 318, 440, 549 and 562. Nanni also serves as a Trustee for the ACI Foundation. His research interests are in construction materials, their structural performance, and their field application.

INTRODUCTION

The use of non-metallic reinforcement, such as fiber-reinforced polymer (FRP) reinforcing bars, has become a viable alternative to address corrosion problems in steel-reinforced concrete (RC) structures. The last few decades have witnessed significant growth in the utilization of FRP bars, primarily in areas where corrosion is a concern¹⁻⁴. Among the available types (i.e., glass, carbon, aramid, and basalt), Glass-FRP (GFRP) bars have gained considerable attention due to their cost advantage over Carbon-FRP bars⁵. While the initial cost of GFRP rebars is often cited as a significant drawback, particularly in comparison to steel rebars, it is noteworthy that the initial cost of GFRP rebars has undergone significant changes over the past two years. These changes are primarily attributed to global price fluctuations in the metal market since the mid-2020s and the concurrent expansion of the GFRP rebar market⁶.

The improvement in material properties, such as the second generation of GFRP bars with a modulus of elasticity of up to 60 GPa (8,700 ksi), coupled with available standards like the new ACI 440.11-22⁷ code and ASTM D8505-23⁸, and the adoption of new construction strategies, enables the exploitation of the complete potential of GFRP rebars for use in concrete structures. However, there are still certain drawbacks for its full implementation as a reinforcement material. The existing development length equation yields large values, leading to challenges in detailing and congestion of bars, particularly at exterior supports⁹. The equation specified in the ACI 440 building code⁷ was derived by Wambeke and Shield¹⁰ using a procedure similar to that employed for steel reinforcement in ACI 318^{11,12}. Nevertheless, due to a lack of comprehensive data on embedment or splice length, conservative assumptions were made, and the influence of certain parameters was disregarded. Since the initial inclusion of the equation in the guidelines, numerous research projects have been dedicated to assessing and refining its accuracy. The findings from these studies present conflicting perspectives regarding the reliability of the current equation in accurately predicting bond strengths. While some researchers argue that the equation produces overly conservative results, others state that it may lead to a potential overestimation of the bond strength^{13–15}.

This paper presents the preliminary results of an experimental study focused on assessing the bond stresses between the new generation of GFRP bars and the surrounding concrete. The specimens comprised under-reinforced concrete beams measuring 300 mm (11.8 in.) in width, 440 mm (17.3 in.) in depth, and 4,800 mm (189 in.) in length, subjected to a four-point bending test. The instrumentation included strain gauges along the rebar and small potentiometers placed at the end of the lap splice, located in the constant moment zone. The results demonstrated that, for the evaluated bar type (i.e., sand-coated surface treatment), the bond primarily arises due to the friction between the surfaces. Although relative slippage was observed in the spliced region, as indicated by the small potentiometers, these displacements appear to have a limited impact on bond strength and stress transfer, as the strain gauges on the bar

exhibited linear behavior until failure. Additionally, the moment-displacement curves indicated that the beam's stiffness remained unaffected, with only its capacity being altered.

BOND STRESSES IN GFRP BARS

Numerous studies have explored the bond behavior of FRP bars in concrete. However, some of these studies have centered around pull-out tests, which might not accurately represent the true stress state in a flexural element. Nevertheless, these tests can provide insights for comparing the performance of surface treatments. Yan et al.⁵ analyzed more than 680 pull-out test specimens and identified various bond failure modes for GFRP bars in concrete, including pullout failure, splitting failure, anchorage failure, rebar fracture, and delamination of resin. Parameters influencing bond strength appeared to include concrete compressive strength, bar size, concrete cover, embedment length, bar spacing, and transverse reinforcements. Solyom and Balázs¹⁶ investigated the impact of surface characteristics on the bond behavior of FRP bars in concrete by conducting pull-out and direct tensile pull-out tests (where the surrounding concrete is in compression) on FRP bars. Their findings indicated that the highest bond strength values were achieved with sand-coated bars, while the lowest was observed with indented ones. Moreover, the study revealed substantial variability in bond strength for a given surface profile; depending on factors like the type, quality, and quantity of sand, the bond strength of sand-coated bars could even double. Pull-out tests carried out by Rolland et al.¹⁷ on sandcoated E-glass/vinylester FRP bars demonstrated an increase in bond strength with larger bar diameters. The authors noted that the size and angularity of sand particles contribute to enhancing the effectiveness of the surface treatment. This raises the question of the impact of surface treatment on the bond strength of GFRP bars, a factor not accounted for in the current ACI 440.11-22⁷ development length equation but addressed in other codes.

A research study by Pay, Canbay, and Frosch¹⁵ reported unconservative results when using the ACI 440.1R-15¹⁸ equation. The results indicated that the bond strength was influenced by the modulus of elasticity and axial rigidity of the reinforcement. They found that the relationship between bond strength and splice length was nonlinear, with deviations from the traditional square root relationship observed for GFRP reinforcement. Surface deformation had minimal impact on bond strength, supporting a common design procedure for various FRP bar types. Furthermore, recent advancements in material properties prompted Ruiz et al.¹³ to question the conservatism of the embedded lengths recommended by ACI 440.1R-15¹⁸. They found that the embedded lengths appeared to be over-conservative (around 55%) when testing sixteen reinforced concrete beams under three-point bending using GFRP bars (sand-coated and helically grooved surfaces). Similarly, Newman et al.¹⁹ conducted an analysis of 48 beams reinforced with GFRP and CFRP, finding that the development length equation in ACI 440 was excessively conservative. Hossain et al.²⁰ compared their experimental data from 96 bond tests to the estimates provided by the bond strength equations in ACI 440, reporting similar results. Additionally, based on 72 pullout tests and 32 beam tests, Ametrano²¹ stated that the development length equations in ACI 440 were also conservative¹⁴.

Recently, Abbas et al.²² Tested eight full scale beams (250 x 400 x 3200 mm) under two-point loads. 2-12mm diameter Ribbed GFRP bars were used with 65d_b splice length. Ready-mix concrete of 45 MPa and 8mm diameter steel stirrups were used. They found that the addition of shear stirrups along the lapped bars prevented cover splitting. The presence of a non-contact lap splice with increased gap between lapped bars improved bond strength, with a maximum increase of 27% observed without shear stirrups. Furthermore, the spacing of shear stirrups also had a significant impact, with an increase in bond strength of 39% and 85% for contact laps and 20% and 44% for lapped bars with a gap, at stirrup spacings of 100mm and 50mm, respectively. They proposed an analytical model to compute the capacity of spliced beams. Wu et al. ²³also found that the presence of stirrups along the splice length increase the bond strength. The performance of the specimen also improved when the stirrups were closer together.

EXPERIMENTAL PROGRAM

Material characterization

The longitudinal reinforcement of the beam specimens comprised an M16 (No.5) GFRP rebar with a nominal diameter of 15.9 mm (0.625 in.) and a nominal area of 199 mm² (0.31 in.²) as per ASTM D8505⁸. The rebar was pultruded using continuous ECR (Electrical Corrosion Resistance) fibers impregnated in a thermosetting vinyl-ester resin, resulting in a mass fiber content of 83%. The surface enhancement of the rebar consisted of a thin sand coating. Table 1 lists the mechanical properties of the reinforcing GFRP bar as determined by tensile tests on representative samples. M16 (No.5) GFRP bars were also utilized as bottom reinforcement to support the reinforcement cage. Similarly, GFRP

M13 (No.4) stirrups were employed as transverse reinforcement throughout, with exception of the constant moment zone.

Table 1	_ Mechanical	characterization	of GERP rebars

Characterization	Standard	Average (μ)	Std Dev (σ)
Fiber mass content	ASTM D2584	83%	0.2%
Glass transition temperature	ASTM E1356	113 °C (235 °F)	9.6 °C (17.2 °F)
Degree of cure	CSA S807	99%	0.3%
Measured cross-sectional area	ASTM D7205	238 mm ² (0.369 in. ²)	3.5 mm ² (0.0054 in. ²)
Ultimate tensile force	ASTM D7205	264 kN (59.3 kip)	6 kN (1.35 kip)
Ultimate tensile strength	ASTM D7205	1326 MPa (192 ksi)	30.1 MPa (4.4 ksi)
Tensile modulus of elasticity	ASTM D7205	64.94 GPa (9416 ksi)	1.065 GPa (154.4 ksi)
Ultimate tensile strain	ASTM D7205	2.04%	0.06%
Ultimate transverse shear force	ASTM D7617	90 kN (20.2 kip)	1.2 kN (0.28 kip)
Ultimate transverse shear strength	ASTM D7617	226 MPa (33 ksi)	3.1 MPa (0.4 ksi)
Moisture absorption (24h)	ASTM D570	0.07%	0.003%

The concrete used for the beam specimens was prepared using a standard structural ready-mixed concrete, specifically designed to achieve a targeted strength of 35 MPa (5070 psi) with coarse aggregate of nominal size of 19 mm (3/4 in.). In order to have improved workability, the concrete slump was approximately 150 mm (6.0 in.). The average compressive strength was measured by testing five concrete cylinders after 28 days according to ASTM C39 ²⁴. A compressive strength of 40.1 MPa (5800 psi) was obtained with a standard deviation of 1.8 MPa (261 psi) (coefficient of variation of 4.5%). The modulus of elasticity of the concrete was computed according to ACI 318-19 based on the 28-day compressive strength: $E_c = 4700\sqrt{f'c}$ (in S.I).

Specimen design

The study consisted of four GFRP-reinforced concrete beams, each measuring 300 mm (11.8 in.) in width, 440 mm (17.3 in.) in depth, and 5,200 mm (205 in.) in length (with a span length of 4,800 mm or 189 in.). To ensure a tension-controlled section (FRP rupture), a concrete compressive strength of 40 MPa (5800 psi) was used, along with one M16 (No.5) GFRP sand-coated bars as longitudinal reinforcement. A concrete cover of 38 mm (1.5 in.) was selected, representing the minimum clear cover for a beam member. Figure 1 shows the reinforcement details of the un-spliced GFRP-RC beam specimen.

Based on the provided data, the expected cracking load, design load, and ultimate expected load was computed using ACI 440.11-22⁷ provisions. The main difference between these calculations is that for determining the design load, all design factors were applied (i.e., environmental reduction factor (C_E), strength reduction factor (ϕ), and the guaranteed tensile strength (f_{fu}) was utilized), while in contrast, when computing the ultimate expected load, these factors were not considered. Instead, the mean tensile strength (f_{u}) from testing was utilized without affecting it by its standard deviation (σ). Before calculating the design moment (nominal moment multiplied by the strength reduction factor), it was necessary to verify that the section was tension-controlled and exhibited a FRP rupture failure, rather than a concrete crushing failure. ACI 440.11-22⁷, in chapter 22.3.1.1 provides guidance for sections in which the GFRP rupture limit state controls the design. There are two possible design approaches. The first is a simplified and conservative bound for the nominal flexural strength, derived from equilibrium of forces and strain compatibility, while assuming that the neutral axis is equal to the balanced neutral axis. The second approach involves a more exact calculation for the neutral axis depth. For the current calculation, the Todeschini Stress-Block method was selected, requiring an iterative process to determine the concrete stress and the neutral axis depth. Given that the section was tension-controlled, a strength reduction factor of 0.55 was used. After multiple iterations, a design moment (ϕ Mn) of 45 kN·m (33.2 kip·ft) and an expected ultimate moment (Mthe) of 100 kN·m (73.8 kip·ft) were determined.

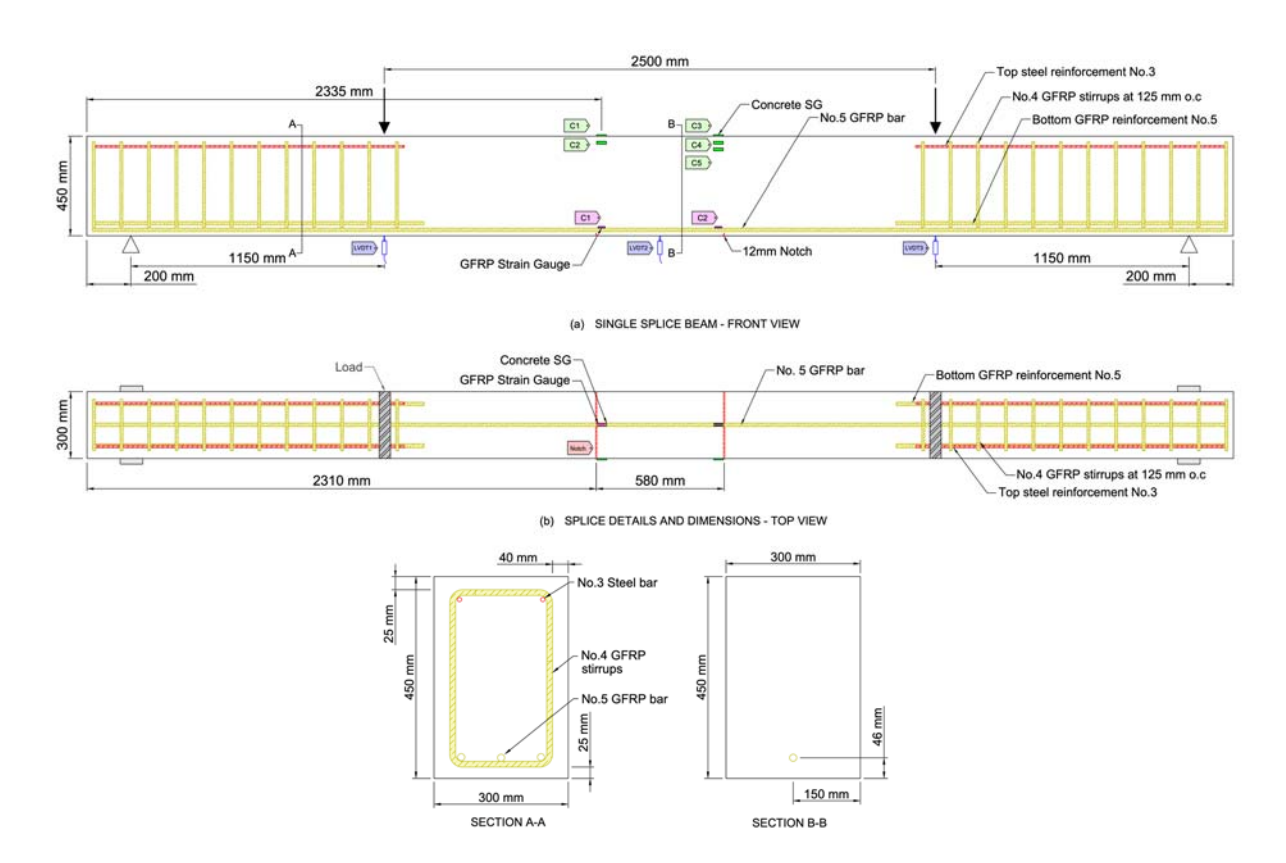


Figure 1 – Reinforcement details of un-spliced specimen; (a) front view; (b) top view; and (c) cross-section views.

Three different lap splices (i.e., 40-, 60- and 80-times bar diameter) were selected based on the available literature. The lap spliced lengths were of 630 mm (25 in.), 950 mm (37.5 in.) and 1270 mm (50 in.), respectively. Figure 2 presents the reinforcement details and dimensions of lap spliced specimens (the figure illustrates a specimen with a splice length of 60 d_b , while all other specimens remain identical except for the variation in splice length). Table 2 presents the specimen details.

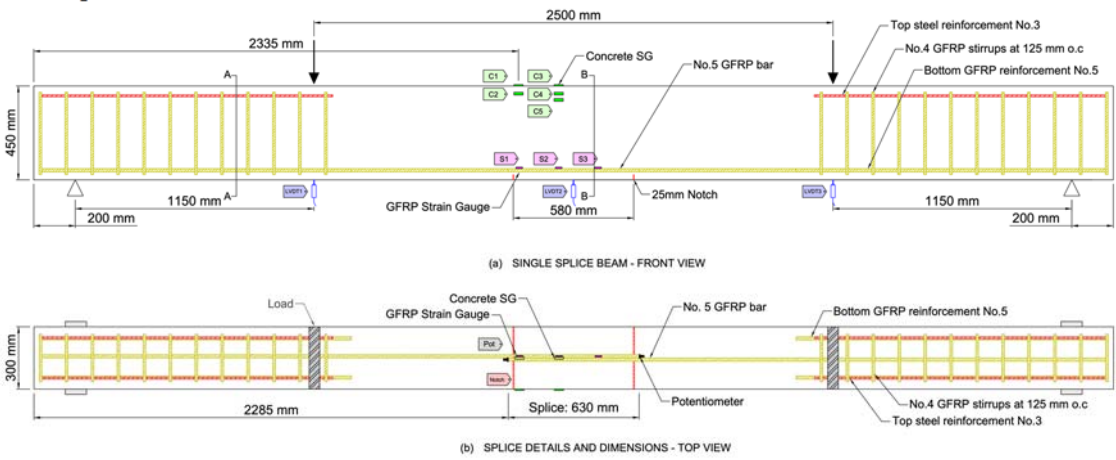


Figure 2 – Reinforcement details of lap-spliced specimens; (a) front view; (b) top view.

Development length requirements

The required development length for a M16 (No.5) GFRP rebar was computed based on ACI 440.11-22 chapter 25.4.2⁷ and shown in Eq. 1.

$$l_d = \frac{\left(\frac{f_{fr}}{0.083\sqrt{f'_c}} - 340\right)\Psi_t}{13.6 + \frac{C_b}{d_b}} d_b \qquad (SI)$$
 (1)

Where:

 f_{fr} = Stress in the bar required to develop the full nominal sectional capacity (MPa). It is equal to f_{fu} for tension-controlled designs and is less than f_{fu} for all other case.

 C_b = Lesser of the distance from center of a bar to nearest concrete surface, and one-half the center-to-center spacing of bars being developed (mm). The ratio between C_b and d_b shall not be taken greater than 3.5.

 Ψ_t = Factor used to modify development length for casting location in tension. It shall be 1.5 if more than 12 in. of fresh concrete is placed below horizontal reinforcement being developed and 1.0 for all other cases.

In addition, the original equation, developed by Wambeke and Shield¹⁰ and shown in Eq. (2, was utilized to compute the spliced length to achieve the full capacity of the rebar.

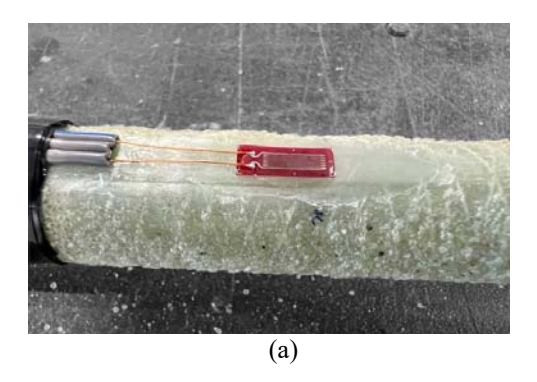
$$l_d = \frac{\left(\frac{f_u}{0.33\sqrt{f'_c}} - 100\right)}{4.0 + \frac{C_b}{d_b}} d_b \qquad (SI)$$
 (2)

Based on above procedure. An embedment length of 109 times the bar diameter or 1.75 m (69 in.) was required to reach the full capacity of the M16 (No.5) GFRP bar. This length was reduced to 100 d_b or 1.60 m (63 in.) when working with ACI 440.11 requirements, such as the implementation of the environmental factor (C_E) and the guaranteed tensile strength (f_{fu}^*). Furthermore, chapter 25.5.2.1 establishes lap splice lengths of GFRP bars in tension, which should be the greater between 1.31_d, 20d_b and 12 in. In this case, the splice length should be 130d_b or 2.05 m (82 in.).

Instrumentation

Throughout the test, data on the load, strains (in both the reinforcement and concrete), and deflection were collected in order to assess the structural behavior of the beam specimens. Mid-span deflection was monitored using a linear variable differential transformer (LVDT) positioned at mid-span and at the points of load application, oriented towards the bottom face of the beam. Strains in both the concrete and the rebar were measured using adhesively bonded strain gauges. All these measuring devices were connected to an independent multi-port data acquisition system, as shown in Figure Figure 3.

Three strain gauges, each with a gauge length of 6 mm, were installed along the length of the rebar before the beam casting. The first strain gauge was positioned 50 mm (2 in.) inside the lap splice end (as shown in Figure 1Figure 2 and Figure 3), and the remaining two were distributed along the splice length, with the second one placed at l_{splice}/3). While installing the strain gauges, efforts were made to minimize any disruption to the sand coating treatment. The installation required the surface to be ground at the application point, which could affect the bond strength of the rebar. This consideration led to the decision to install only three strain gauges along the length of the rebar. Lastly, once the concrete had hardened and the beams were ready for testing, five strain gauges with gauge length of 60 mm were placed to the upper part of the beams to monitor compressive strains in the concrete.



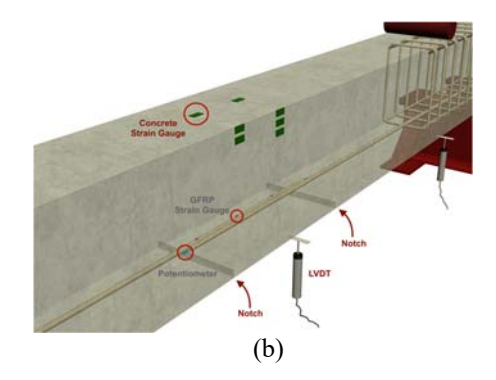
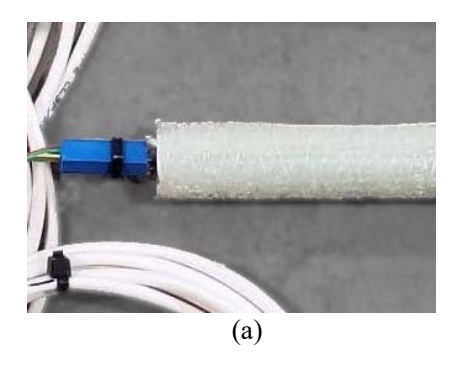


Figure 3 – Instrumentation (a) Strain gauges installation; (b) Instrumentation detailing.

Additionally, a small potentiometer was positioned at the center of the rebar cross-section to measure relative slip. The procedure employed was both straightforward and effective. A small hole was drilled at the center of the rebar, with ample tolerance to accommodate the potentiometer shaft (refer to Figure 4). Before inserting the shaft into the hole, resin was carefully applied to ensure good adhesion. Subsequently, the potentiometer was covered with a heat shrink tube to protect against potential damage during concrete pouring and to ensure its stability. Once the reinforcement cage was positioned within the formwork, the potentiometer was securely fastened to prevent any movement along with the rebar.



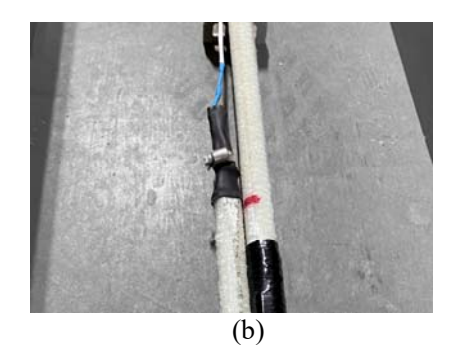


Figure 4 – Potentiometers installation (a) In rebar; (b) With heat shrink tube.

Test setup

The four-point-bending beams were tested using a displacement control protocol at a rate of 1.2 mm/min, comprising three cycles. During the first cycle, the beams were loaded up to 1.15 times the calculated cracking load. In the second cycle, the beams were loaded up to the calculated design load or until a rebar slippage of 0.5 mm occurred, whichever happened first (this slippage value was selected based on a literature review as a reference for rebar movement). Lastly, the third cycle continued until the beams reached failure. Before testing, a 25 mm (1 in.) notch was made in each beam near the end of the splice to induce main cracks specifically at the lap splice location (refer to Figure 1 & Figure 2 for reference). Figure 5 depicts the schematic setup of the four-point bending test.



Figure 5 – Test setup illustration.

RESULTS AND DISCUSSION

The results obtained from the four-point bending tests are presented in Table 2. The table includes the ratio between the experimental moment and the theoretical moment, as well as the experimental-to-design moment ratio. Notably, the un-spliced GFRP-RC beam nearly reached the expected moment before failure, surpassing the design moment by 119%. Although this specimen was intended to be an under-reinforced member with the expected failure mode of "FRP rupture", it ultimately failed due to concrete crushing near the point of load application. However, an analysis of the strain gauges positioned near the notches on the bar revealed a maximum strain of approximately 0.019, equivalent to 93% of the ultimate tensile strain. This indicates that the bar was close to rupture. Regarding the lapspliced specimens, they all failed before reaching the expected capacity. Nevertheless, they each exceeded the design moment. For instance, SL40, which had a lap splice length of $40d_b$ or 630 mm (32% the required lap splice length), surpassed the design moment by 6%, as shown in Table 2. This shows the conservatism of the design philosophy.

Table 2 – Specimen details and test result	Table 2 – S	pecimen	details	and	test res	ults
---	-------------	---------	---------	-----	----------	------

Specimen ID	Lap Splice Length	f'c (MPa)	Mid-span deflection	Test moment (M _{exp})	M_{exp} / M_{the}	M_{exp} / ϕM_n	Failure mode
un-spliced	un-spliced	35.5	131 mm (5.1 in.)	96 kN·m (71 kip·ft)	0.96	2.19	Concrete crushing
SL40	40 d _b (630 mm)	40.0	46 mm (1.8 in.)	47 kN·m (35 kip·ft)	0.46	1.06	Splitting
SL60	60 d _b (950 mm)	43.0	72 mm (2.8 in.)	61 kN·m (45 kip·ft)	0.61	1.39	Splitting
SL80	80 d _b (1270 mm)	42.1	78 mm (3.1 in.)	73 kN·m (54 kip·ft)	0.72	1.65	Splitting

Failure mode

The observed failure mode in all lap-spliced specimens was identified as splitting, attributed to a distinct bottom crack that extended along the length of the splice. This crack influenced the stress transfer mechanism, causing the surrounding concrete to separate from the rebar and ultimately leading to a reduction in the overall load-bearing capacity of the beam. Figure 6 illustrates the specimens after testing, showcasing the effects of this failure mode. In comparison to the un-spliced specimen, where the cracks appear to be more uniformly distributed and of the same width, it is evident that the spliced specimens exhibited main cracks at the splice end, disrupting this uniform distribution. The initial group of cracks occurred at the notches, emerging at an approximate moment of 26 kN·m (19.2 kip·ft), and then propagated while widening towards the upper face of the beam.

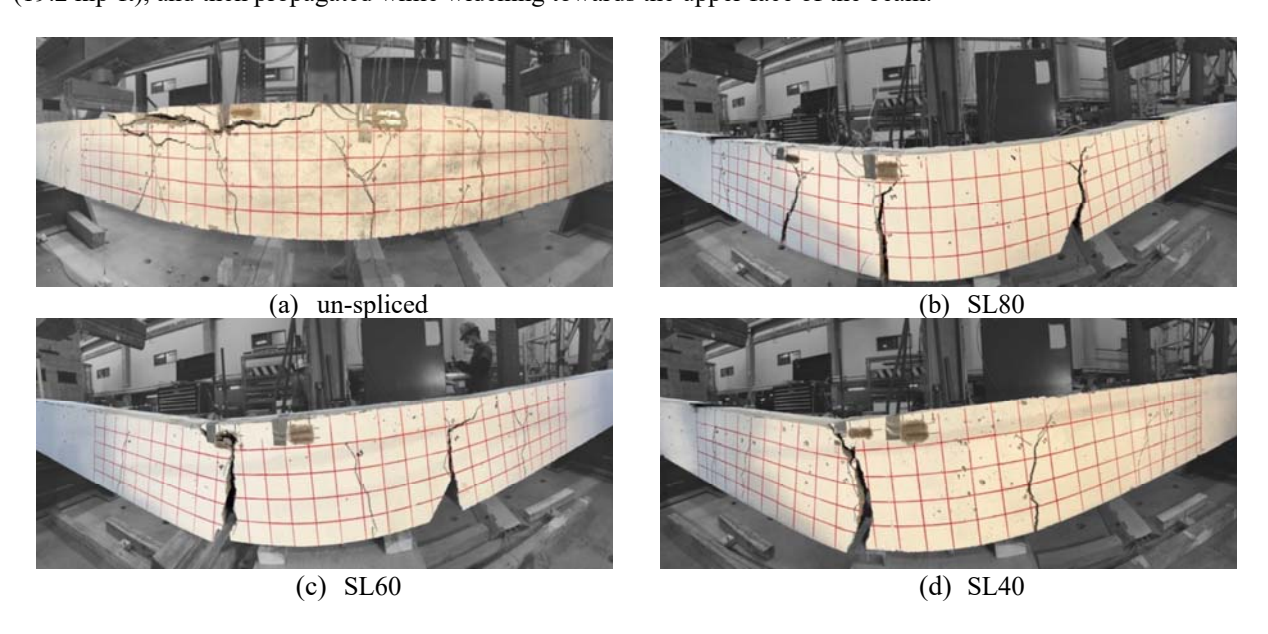


Figure 6 – failure mode of the specimens.

Moment-Deflection Curve

Figure 7 illustrates the mid-span moment versus deflection curves for all the tested specimens. Highlighting the maximum capacity of each specimen, as well as the expected and design moments. Upon examining the figure, it became evident that while the capacity of the lap-spliced specimens was lower compared to the un-spliced one, this discrepancy had a minimal impact on the stiffness of the beam. Although the cracking moment influenced the point of change in slope, it was apparent that they exhibit similar stiffness thereafter. This might suggest that the relative movement of the surrounding concrete did not significantly affect the bond capacity of the beam. The rebar remained capable of carrying load until it reached a maximum slippage value, indicating its ability to maintain load-bearing capacity. These observations lead to the inference that the bond capacity between the rebar and surrounding concrete remained almost intact, enabling load transfer even with some relative movement. In summary, SL80, SL60 and SL40 specimens reached an ultimate moment of 76%, 64% and 49% of the un-spliced specimen moment, respectively. In terms of deflection, the lap-spliced specimens reached the 60%, 55% and 35% of the maximum deflection of the un-

spliced specimen. One might have expected a greater deflection in the lap-spliced specimens due to the potential for rebar slippage and the widening of the main crack. However, it appears that, even though the distribution of cracks differed from that in the un-spliced specimen, the nonuniform crack pattern still resulted in a similar level of deflection when subjected to the same applied load. In a scenario of bond failure, the specimen might not exhibit excessive deflection as an early indicator of design failure. The warning signs of bond failure would manifest as localized cracks at the lap splice end, distinguishable by their wider width compared to the other cracks distributed along the beam. It is noteworthy that even though a 68% reduction in the required lap splice length would lead to bond failure, the capacity of the specimen would still exceed the design moment requirements.

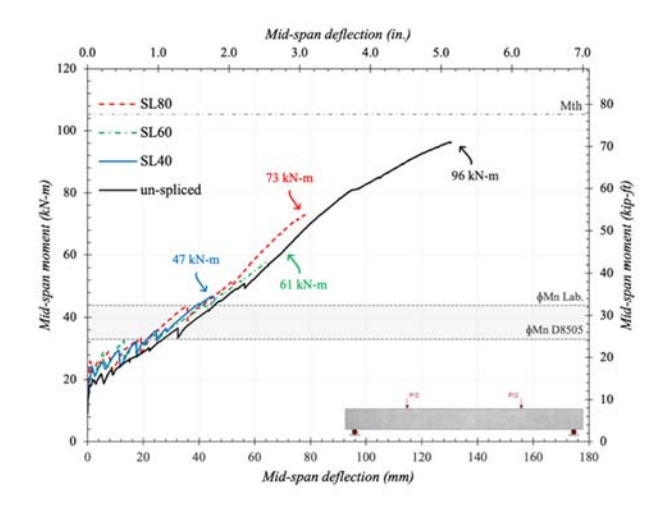


Figure 7 – Mid-span moment vs deflection curves.

Bond strength

The analysis of mid-span moment versus deflection revealed that the bond strength of the rebar remained unaffected. Figure 8 presents the behavior of a potentiometer installed at the end of the rebar in the SL80 specimen, showing continued movement of the rebar after the initial beam cracking. The specimen was able to continuously carry the applied load. It was anticipated that the member's stiffness would decrease after rebar slippage, resulting in a greater deflection. However, the green curve and previous evidence indicated that the movement of the rebar did not significantly impact its bond capacity until it experienced a slippage of approximately 4.3 mm (0.17 in.). Nonetheless, it is important to note that these findings may not apply to other specimens, as the potentiometer readings demonstrated smaller slippage values with decreasing splice length, suggesting potential variations in rebar behavior and bond capacity in different scenarios. SL40 specimen reached a maximum slippage of around 2.0 mm (0.08 in.) before failure. It seems that the larger the lap splice length, the greater the capacity of resist movement before a brittle failure.

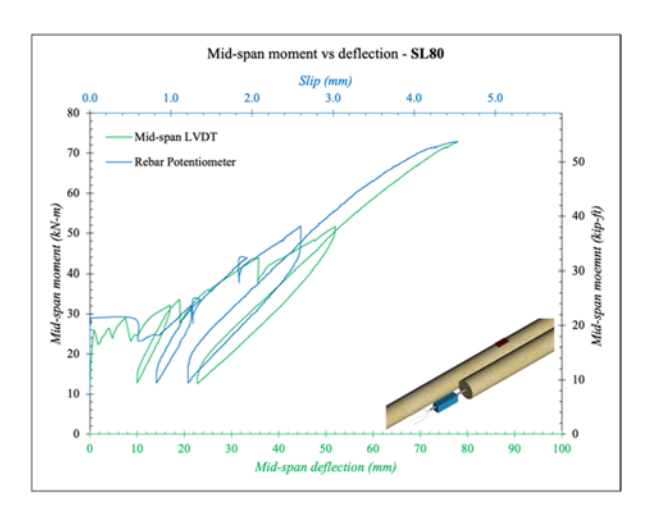


Figure 8 – Mid-span moment vs deflection with potentiometer.

The calculation of maximum bond stress in the rebar is challenging due to the unknown distribution of bond stresses along its length. Consequently, it is common practice to calculate the average bond stress along the splice length. In Table 3, column 3, the maximum bond values based on ACI 440.11-22⁷ for each splice length are presented. Additionally, column 4 displays the average bond strength calculated using the maximum strain at failure. A comparison of the bond stress ratios revealed a close correspondence between the computed values and those recommended by ACI, indicating that ACI provides reliable estimates for bond stresses under the assessed parameters (i.e., avoiding the effect of the confining reinforcement). Figure 9 further illustrates the bond stress values of the specimens in comparison to both ACI and the average expected value, visually demonstrating the agreement between computed and expected bond stresses.

T 11 3	a .	1	1		1	
Table 3 -	 Snecimen 	details	and	test	resu	ts

Specimen ID	Splice Length	U _{ACI}	Uavg	U _{ACI} / uavg
un-spliced	un-spliced	-	-	-
SL40	40 d _b (630 mm)	3.9 MPa (561 psi)	3.8 MPa (550 psi)	1.020
SL60	60 d _b (950 mm)	3.4 MPa (496 psi)	3.3 MPa (482 psi)	1.030
SL80	80 d _b (1270 mm)	3.2 MPa (466 psi)	3.0 MPa (431 psi)	1.081

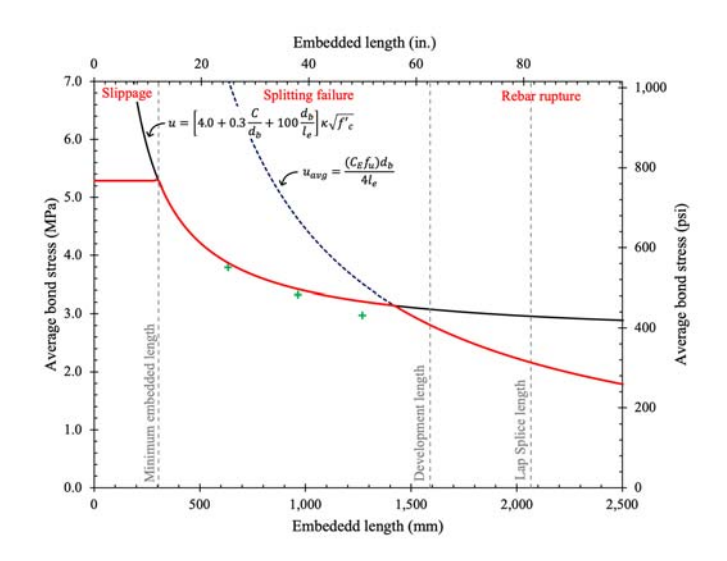


Figure 9 – Bond stresses in rebars.

CONCLUSIONS

Four full-scale beam specimens were tested under four-point bending to evaluate and analyze the bond stresses of a new generation GFRP sand-coated bar (M16 (No.5) designation). Three different lap splice lengths were assessed (i.e., 40-, 60-, and 80-d_b) without any confinement effect. A small potentiometer was installed in the rebars to measure the relative slippage. Based on the findings the following conclusions can be drawn.

1. The un-spliced GFRP-RC beam exhibited a failure mode of concrete crushing near the point of load application, rather than the expected FRP rupture failure. Nevertheless, the strain gauges positioned near the notches on the GFRP bar indicated that it was close to rupture, having reached approximately 93% of the ultimate tensile strain. Furthermore, the lap-spliced GFRP-RC specimens failed due to splitting, where a bottom longitudinal crack led to the surrounding concrete separating from the rebar, resulting in a loss of bearing capacity.

- 2. The lap-spliced GFRP-RC specimens exceeded their design moments based on ACI 440.11-22 requirements, indicating that even though they did not reach the maximum capacity, from a design perspective the specimens could performance in an efficient way. For example, the SL40 specimen with a splice length of 40db (630 mm) surpassed its design moment by 6%.
- 3. The stiffness of the lap spliced specimens was comparable to that of the un-spliced beam, indicating that relative movement of the surrounding concrete did not significantly affect the bond performance between the GFRP bar and the concrete. The rebar was able to maintain load-bearing capacity even with some slippage, suggesting that the bond performance remained intact up to a certain level where a brittle failure occurred.
- 4. The average bond stress calculated along the lap splice length closely matched the maximum bond stress values predicted by the ACI 440.11-22 equation. This alignment suggests that, under these reinforcement and detailing conditions, the equation can accurately predict the maximum bond stress.

ACKNOWLEDGMENTS

We gratefully acknowledge the members of the Integrated Research Laboratory for the Development of Materials and Sustainable and Innovative Structures at the University of Sherbrooke in Canada, particularly Jérôme, Steven and Pascal for their invaluable support and assistance throughout the fabrication and testing process. Furthermore, to the Department of Civil and Architectural Engineering at the University of Miami for their significant contribution to this study. The authors gratefully acknowledge the financial support from the National Science Foundation IU-CRC Center for Integration of Composites into Infrastructure (CICI) under grant #1916342.

REFERENCES

- Nanni, A., de Luca, A., and Jawaheri Zadeh, H. "Reinforced Concrete with FRP Bars: Mechanics and Design," CRC Press. 2014.
- 2. Ekenel, M., y Basalo, F. D. C., and Nanni, A. "Fiber-Reinforced Polymer Reinforcement for Concrete Members," *Concrete International*, V. 43, No. 2, 2021, pp. 18–22.
- 3. Salan, A. V., Rahman, M. K., Al-ghamdi, S., et al. "A Monumental Flood Mitigation Channel in Saudi Arabia," *Concrete International*, No. October, 2021, pp. 33–41.
- 4. Classen, M., Hegger, J., Bielak, J., et al. "Shear capacity of continuous concrete slabs with CFRP reinforcement," V. 320, 2022.
- 5. Yan, F., Lin, Z., and Yang, M. "Bond mechanism and bond strength of GFRP bars to concrete: A review," *Composites Part B: Engineering*, V. 98, 2016, pp. 56–69.
- 6. Ortiz, J. D., Khedmatgozar Dolati, S. S., Malla, P., et al. "FRP-Reinforced/Strengthened Concrete: State-of-the-Art Review on Durability and Mechanical Effects," *Materials*, V. 16, No. 5, 2023.
- 7. ACI Committee 440. "Code Requirements for Structural Concrete Reinforced with Glass FRP Bars (ACI 440.11-22)," American Concrete Institute, Farmington Hills, MI., 2022.
- 8. ASTM Committee D30. "D8505-23, Standard Specification for Basalt and Glass Fiber Reinforced Polymer (FRP) Bars for Concrete Reinforcement," ASTM International, West Conshohocken, PA. USA, 2023.
- 9. Hussain, Z., and Nanni, A. "Design and Detailing of Glass Fiber-Reinforced Polymer-Reinforced Concrete Beams according to ACI 440.11-22," *ACI Structural Journal*, 2023.
- 10. Wambeke, B. W., and Shield, C. K. "Development length of glass fiber-reinforced polymer bars in concrete," *ACI Structural Journal*, V. 103, No. 1, 2006, pp. 11–7.
- 11. ACI Committee 318. "Building Code Requirements for Structural Concrete and Commentary (ACI 318-19)," American Concrete Institute, Farmington Hills, MI., 2019.
- 12. Orangun, C. O., Jirsa, J. O., and Breen, J. E. "A Reevaluation of Test Data on Development Length and Splices," *ACI Journal Proceedings*, V. 74, No. 3, 1977, pp. 114–22.
- 13. Ruiz Emparanza, A., De Caso, F., and Nanni, A. "Development Length of GFRP Rebars in Reinforced Concrete Members under Flexure," *ACI Symposium Publication*, V. 356, 2022.
- 14. Basaran, B., Kalkan, I., Bergil, E., et al. "Estimation of the FRP-concrete bond strength with code formulations and machine learning algorithms," *Composite Structures*, V. 268, No. February, 2021, p. 113972.
- 15. Pay, A. C., Canbay, E., and Frosch, R. J. "Bond strength of spliced fiber-reinforced polymer reinforcement," *ACI Structural Journal*, V. 111, No. 2, 2014, pp. 257–66.
- 16. Solyom, S., and Balázs, G. L. "Bond of FRP bars with different surface characteristics," *Construction and Building Materials*, V. 264, 2020, p. 119839.

- 17. Rolland, A., Quiertant, M., Khadour, A., et al. "Experimental investigations on the bond behavior between concrete and FRP reinforcing bars," *Construction and Building Materials*, V. 173, 2018, pp. 136–48.
- 18. ACI Committe 440. "Guide for the Design and Construction of Structural Concrete Reinforced with Fiber-Reinforced Polymer (FRP) Bars (ACI 440.1R-15)," American Concrete Institute, Farmington Hills, MI., 2015.
- 19. Newman, N., Ayoub, A., and Belarbi, A. "Development length of straight FRP composite bars embedded in concrete," *Journal of Reinforced Plastics and Composites*, V. 29, No. 4, 2010, pp. 571–89.
- 20. Hossain, K. M. A., Ametrano, D., and Lachemi, M. "Bond Strength of Standard and High-Modulus GFRP Bars in High-Strength Concrete," *Journal of Materials in Civil Engineering*, V. 26, No. 3, 2014, pp. 449–56.
- 21. Ametrano, D. "Bond characteristics of glass fibre reinforced polymer bars embedded in high performance and ultra-high performance concrete." Ryerson University, Toronto, 2011.
- 22. Abbas, H., Elsanadedy, H., Alaoud, L., et al. "Effect of confining stirrups and bar gap in improving bond behavior of glass fiber reinforced polymer (GFRP) bar lap splices in RC beams," *Construction and Building Materials*, V. 365, 2023.
- Wu, C., Hwang, H. J., and Ma, G. "Effect of stirrups on the bond behavior of lap spliced GFRP bars in concrete beams," *Engineering Structures*, V. 266, 2022.
- 24. ASTM Committee C09. "C39/C39M-21, Standard Test Method for Compressive Strength of Cylindrical Concrete Specimens," ASTM International, West Conshohocken, PA. USA, 2021.